J. Electrochem. Sci. Eng. **14(2)** (2024) 163-175; http://dx.doi.org/10.5599/jese.2096

Open Access : : ISSN 1847-9286
www.jESE-online.org

Original scientific paper

Cobalt and copper-based metal-organic frameworks synthesis and their supercapacitor application

Sneha Tomar and Vinod Kumar Singh✉

Department of Chemical Engineering, National Institute of Technology Raipur, Raipur, Chhattisgarh, 492001, India

Corresponding author: ✉vksingh.che@nitrr.ac.in

Received: September 25, 2023; Accepted: January 16, 2024; Published: February 11, 2024

Abstract

*In this study, two different metal-organic frameworks (*MOFs*) were synthesized using copper and cobalt metal ions with benzenedicarboxylic acid (bdc) as a common ligand. The prepared MOFs were characterized using X-ray diffraction, Fourier transform infrared spectroscopy, and scanning electron microscopy-energy dispersive spectroscopy. Also, the electrochemical characteristics were analyzed using cyclic voltammetry, galvanostatic charge/discharge, and electrochemical impedance spectroscopy methods. Structural characterizations indicate that Co-bdc MOF is composed of three-dimensional non-uniform colloids and Cu-bdc MOF has a regular three-dimensional cuboidal structure, possessing good crystalline structure. The Cu-bdc MOF exhibited a maximum specific capacitance of 171 F/g, while Co-bdc MOF showed 368 F/g at the current density of 1 A/g. The solution resistance for the Co-bdc MOF was 0.09 Ω in comparison to 1.25 Ω for the Cu-bdc MOF. Also, the Co-bdc MOF demonstrated better cycling performance by retaining 85 % of its capacity after 2000 charge-discharge cycles. In contrast, the stability of the Cu-bdc MOF was lower, with only 78 % retention in capacity. Conclusively, the Co-bdc MOF demonstrated superior specific capacitance, lower resistance, and enhanced cyclic stability in 3 M KOH electrolyte system.*

Keywords

Solvothermal synthesis; benzene dicarboxylic acid ligand; energy storage; specific capacitance

Introduction

The energy crisis has spurred the exploration and development of new energy stockpiling and storage technologies to address issues related to energy supply and demand fluctuations. Renewable energy sources, such as solar and wind, are intermittent. They do not produce a consistent and predictable amount of energy throughout the day. Energy storage allows excess energy generated during peak production times to be stored for later use, smoothing out fluctuations in energy supply.

Supercapacitors (SCs) are considered promising energy storage devices for future applications due to their numerous characteristics, such as long cycling capability, ability to deliver high power, and exceptional reversibility [1]. SCs have successfully entered commercialization because of their exceptional performance characteristics, which are benefited by the physical and chemical characteristics of the active material. SCs assembly mainly consists of anode and cathode electrodes that are immersed in electrolyte (aqueous and nonaqueous) and separated by separators that allow the free flow of ions and electrons [2]. The electrode material plays a crucial role in determining the electrochemical performance of supercapacitor electrodes. It directly influences the overall performance and characteristics of the electrode. The choice of electrode material affects important factors such as capacitance, charge/discharge rates, cycling stability, and overall energy storage capabilities of the supercapacitor [3]. The materials commonly employed in supercapacitor applications include graphene (graphene quantum dots or rGO) [4,5], carbon nanotubes [6], metal oxides (such as NiO, Mn_3O_4, RuO_2) [7-9], transition metal carbides [10], metal-organic frameworks [11], hybrid, and composite materials. Thus, the careful selection of electrode material is crucial for attaining the best possible electrochemical performance for supercapacitors.

Metal-organic frameworks (MOFs) are widely recognized as highly suitable electrode materials for energy storage applications. This is primarily due to their inherent qualities, such as stability, flexibility, structural versatility, and other essential properties [12-14]. MOFs, or porous coordination polymers, are created using the principles of coordination chemistry. In the process of self-assembling, multitopic organic ligands and metal ions, commonly referred to as secondary building units, result in the development of MOFs. In most studies, the solvothermal technique is used to prepare MOFs as it is a simple and cost-effective technique, like microwave-assisted synthesis, sono-chemical synthesis, or electrochemical synthesis [15-18].

In this study, two distinct MOFs were synthesized using different metal salts while employing a common ligand using the solvothermal method. The prepared MOFs were Co-bdc and Cu-bdc MOF (Co: cobalt, Cu: copper, bdc: benzenedicarboxylic acid). Professor O. M. Yaghi and his research group [19] initially identified Co-bdc MOF in 2005, and they designated it as MOF-71. The framework structure comprises endless chains of CoO_6 octahedra, where each chain shares corners. These chains are interconnected with four parallel chains through the bdc linkers. It has attracted noteworthy attention in the field of water splitting [20], supercapacitors [20], sensors [21], and catalysis [22]. Cu-bdc MOF (CCDC no. 687690) is identified by its two-dimensional structure. It is composed of copper ions serving as a metal ion source and 1,4-benzenedicarboxylic acid acting as the bridging organic ligand [23]. It has drawn considerable interest in the domain of Li-ion battery [24], catalyst [25,26], methane storage [27] and adsorption [28]. Both MOFs have been utilized in supercapacitors, and specific details are outlined in Table 1, including a comparative analysis of this study.

Table 1. *Cu and Co-based MOFs and their respective specific capacitance values*

MOF	Ligand	Synthesis method	Electrolyte	Specific capacity, F/g	Ref.
Cu-MOF/rGO	3,3',5,5'-tetracarboxy-diphenylmethane	Solvothermal	1 M Na_2SO_4	21 at 1 A/g	[29]
Cu-MOF/rGO	5,5'-(piperazine-1,4-diyl) di isophthalic acid	Slow evaporation	3 M KCl	135 at 1 A/g	[30]
Cu-MOF/rGO	Benzene-1,3,5-tri-carboxylic acid	Solvothermal	1 M Na_2SO_4	4.1 at 0.8 A/g	[31]

MOF	Ligand	Synthesis method	Electrolyte	Specific capacity, F/g	Ref.
PANI/Cu-MOF	Benzene-1,3,5-tri-carboxylic acid	Co-precipita-tion at room temperature	6 M KOH	459 at 50 mV/s	[32]
Cobalt MOF	Trimesic acid	Solvothermal	1 M KOH	280	[33]
Copper MOF				228	
Copper MOF	Benzene-1,3,5-tri-carboxylic acid	Solvothermal	3 M KOH	228 at 1.5 A/g	[34]
Graphene/ Cu-MOF	Benzene-1,3,5-tri-carboxylic acid	Solvothermal	6 M KOH	190 at 10 mV/s	[35]
Co-MOF	Polycarboxylic acid ligand based tritopic ligand	Solvothermal	1 M tetraethylam-monium tetrafluoro-borate in acetonitrile	300 at 1 A/g	[36]
Co-MOF/ graphene nanosheets	Benzene-1,3,5-tri-carboxylic acid	Precipitation at room temp	1 M KOH	187.3 at 0.25 A/g	[37]
Co-based MOF/graphene nanocomposite	2-methylimidazole	Precipitation at room temperature	6 M KOH	260 at 10 mV/s	[38]
Cu-bdc MOF	Benzene dicarboxylic acid	Solvothermal	3 M KOH	368 at 1 A/g	This work
Co-bdc MOF				171 at 1 A/g	

Experimental

Chemicals and reagents

The reagents and chemicals that were used in the present study were cupric nitrate trihydrate (Loba Chemie, 99.5 %), cobaltous nitrate hexahydrate (Qualigens Thermo Fischer, 97 %), benzene dicarboxylic acid (Merck, ≥98 %), dimethyl formamide (Merck, 99.8 %), polytetrafluoroethylene (PTFE), N-methyl pyrrolidone, and acetylene carbon black. All experiments were conducted using deionized water.

Characterization techniques

Fourier transform infrared spectroscopy (FTIR), Bruker Alpha Model spectrometer was used to examine the secondary structure and functional groups present in Cu-bdc and Co-bdc MOF. X-ray diffraction (XRD), a PANalytical 3 kW X'pert diffractometer outfitted with Ni-filtered CuK radiation was used to examine the patterns of the samples. The morphology and elemental composition of the material were determined using scanning electron microscopy (SEM, Zeiss Evo, Evo18) and energy dispersive spectroscopy (EDS, INCA 250 EDS with X-MAX 20mm Detector).

Synthesis of cobalt- and copper-bdc metal-organic frameworks

Co-bdc MOF was synthesized using 2 mmol of cobalt nitrate salt and 1 mmol of benzene dicarboxylic acid in 50 ml of dimethyl formamide solution. The solution was agitated for 30 minutes to achieve a homogeneous mixture. Then, the resulting solution was transferred into a Teflon-lined autoclave and maintained at 150 °C for 12 hours. The obtained precipitate was subsequently washed three times with ethanol (30 ml) to eliminate impurities and then dried at 50 ˚C for 6 h in hot air oven. Cu-bdc MOF was synthesized using the same method as Co-bdc MOF, with the only difference being the use of cupric nitrate salt instead of cobalt nitrate salt in the synthesis process, as demonstrated in Scheme 1.

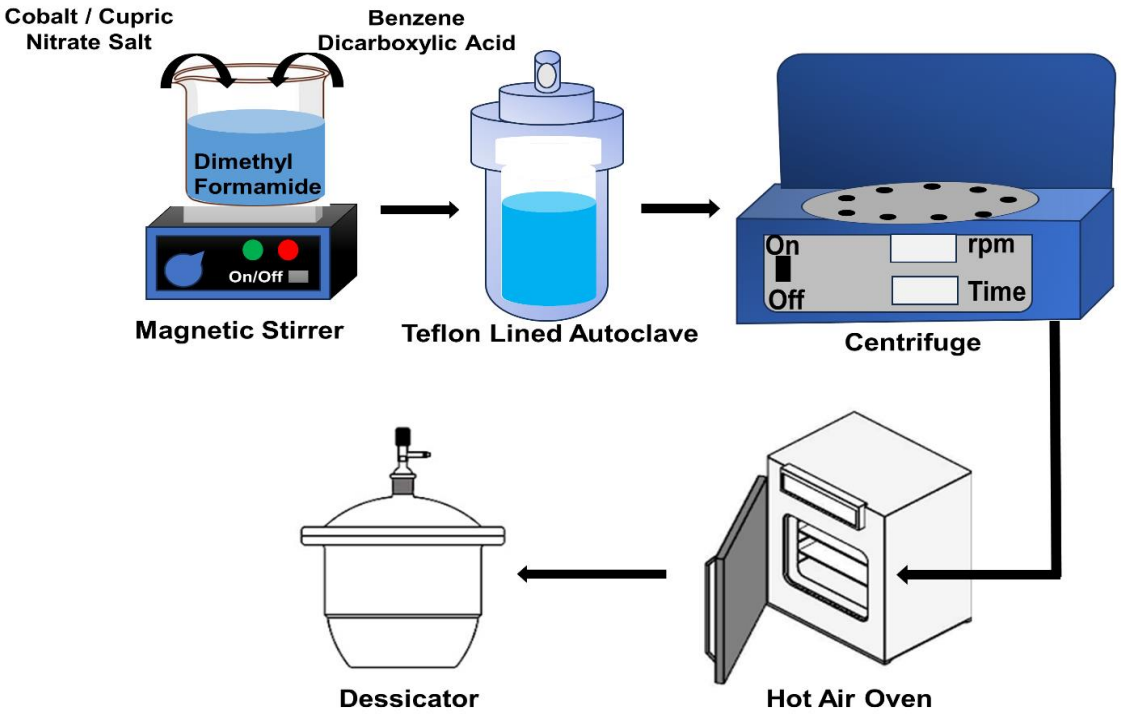

Scheme 1. *Schematic representation of the synthesis procedure for Co-bdc and Cu-bdc MOFs*

Electrochemical measurements

Electrochemical workstation was used to conduct several experiments such as electrochemical impedance spectroscopy (EIS), cyclic voltammetry (CV), galvanostatic charge-discharge (GCD) and cyclic stability in 3 M KOH electrolyte. In the experimental setup, the working electrode consisted of nickel foam coated with the MOF material. The reference electrode used was silver/silver chloride, which provides a stable reference potential for electrochemical measurements. The counter electrode, on the other hand, was a platinum wire, which facilitates the flow of current in the electrochemical cell and completes the circuit. The 3 M KOH solution was used as an electrolyte for the Co-bdc and Cu-bdc electrodes.

The working electrode slurry was a mixture of the active material (Co-MOF or Cu-MOF), conductivity agent (acetylene carbon black), and PTFE binder in the weight ratio of 80:15:5. The pieces of nickel foam (size 1×1 cm) were taken and the slurry was applied layer by layer to achieve the mass loading of 1.2 mg/cm ^{2}. The coated nickel foam pieces were dried under vacuum at 60 ˚C for 24 h to get the working electrode. An EIS study was conducted within a frequency range of 100 kHz to 0.01 Hz, using a 10 mV amplitude. Additionally, CV analysis was performed on Co-bdc MOF within a potential range of -0.5 to 0 V, while for Cu-bdc MOF, the potential range was -0.5 to 0.5 V. The CV measurements were carried out at various scan rates ranging from 10 to 50 mV/s. GCD of MOF electrodes was done for the same potential window as CV at different current densities ranging from 1 to 18 A/g. The cyclic stability test was carried out up to 2000 cycles at 18 A/g.

Results and discussion

Scanning electron microscopy - energy dispersive spectroscopy

Scanning electron microscopy-energy dispersive spectroscopy (SEM-EDS) analysis reveals the morphology and elemental composition of both MOF samples. In the case of the Co-bdc MOF, Figure 1(a) and 1(b) demonstrates non-uniformity among particles, with predominant elements being

cobalt, carbon, and oxygen. Conversely, the Cu-bdc MOF exhibits a well-defined cuboidal morphology, indicating successful structure formation, as depicted in Figure 1(c). By displaying EDS analysis, Figure 1(d) for the Cu-bdc MOF confirms the presence of copper, carbon, and oxygen, thus supporting the successful synthesis of MOFs.

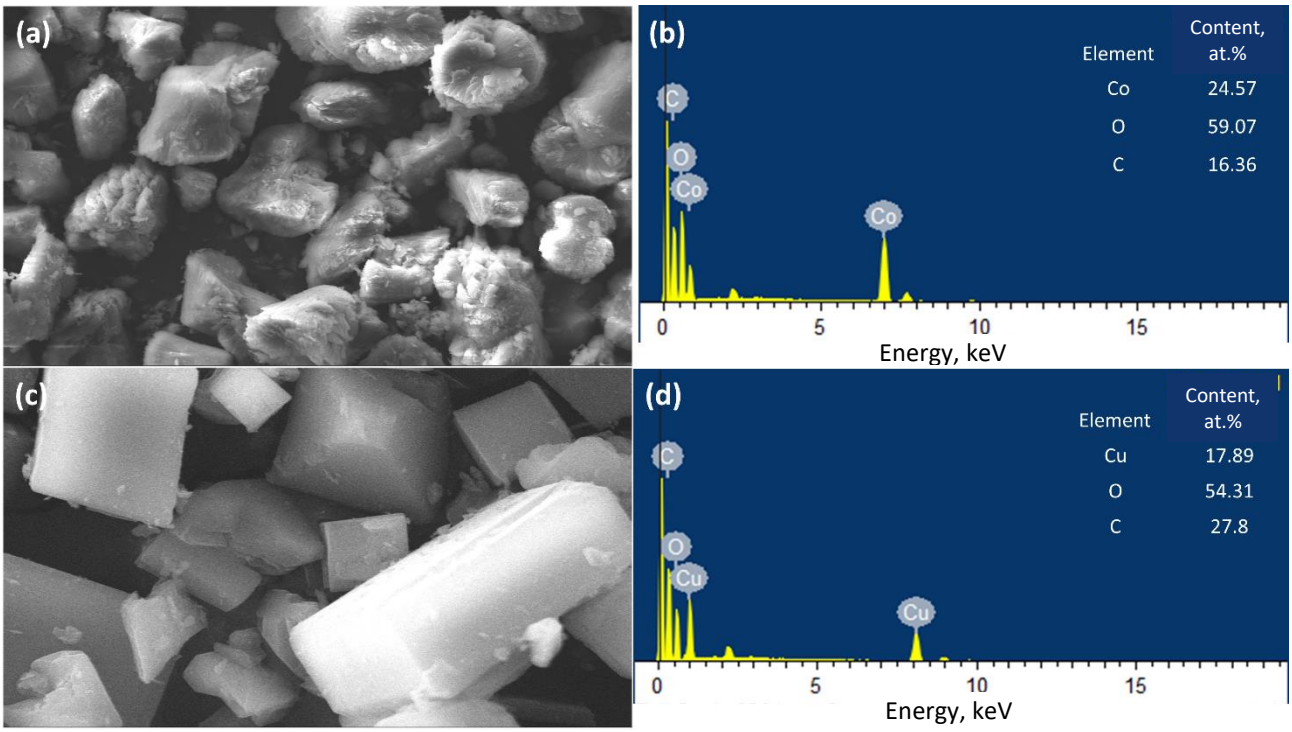

***Figure 1**. SEM-EDS images of Co-bdc MOF (a and b) and Cu-bdc MOF (c and d)*

X-ray diffraction

The geometry used for the powder sample analysis was a Bragg-Brentano. The test conditions were Cu-Kα source, acceleration voltage 40 kV, acceleration current 30 mA, scan speed 0.032 s per step, step interval 0.026° and scan range 5 to 60°. Co-bdc MOF diffraction peaks were located at 2θ values of approximately 8.8, 11.5, 12.0 and 15.9° representing the diffraction planes of (100), (110), (101), and (200), respectively [39] (Figure 2).

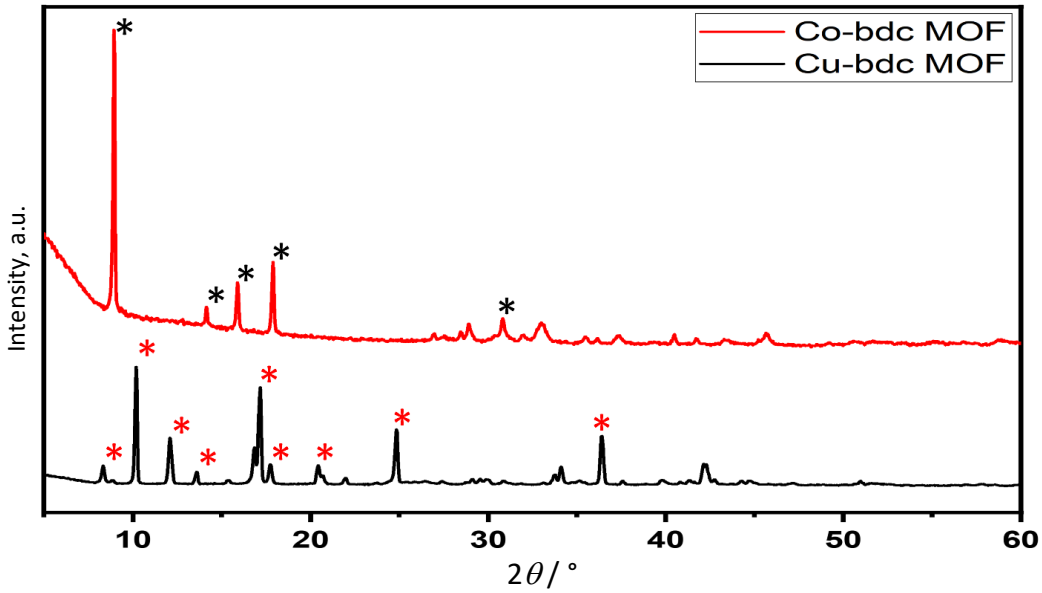

***Figure 2.** XRD patterns of Co-bdc MOF and Cu-bdc MOF*

The peaks at angles of 10.2, 12.05, 13.5, 17.1, 17.6, 20.5 and 24.77° correspond to the lattice planes (110), (220), (020), (333), (211), (202), and (222) of the Cu-bdc MOF. These peaks confirm the successful production of a highly crystalline crystal with strong intensity and strong peaks, which indicate excellent crystalline characteristics of both MOFs (Figure 2). The intensity of the diffraction pattern suggests that the synthesized MOF crystal exhibits a well-organized structure. Additionally, it is observed that the Co-bdc and Cu-bdc XRD patterns are dissimilar due to variations in the metal coordination geometry [40,41].

Fourier-transform infrared spectroscopy

Fourier-transform infrared spectroscopy (FTIR) analysis of Cu-bdc and Co-bdc MOFs is displayed in Figure 3. Cu-bdc underwent FTIR, and the spectrum is shown in Figure 3(a). The interaction between the Cu metal and BDC ligands is validated by the existence of the -COO- group, designated by two bands at 1566 and 1370 cm^{-1}, corresponding to the antisymmetric and symmetric stretch modes, respectively [43]. At 1447 and 2988 cm^{-1}, the C-C and C-H of benzene from benzene dicarboxylic acid were seen, respectively. The spectrum also contained the Cu-O band at 581 cm^{-1} in addition to the BDC [43]. Figure 3(b) shows that the sharp peak at 3700 cm^{-1} originates from OH bound to BDC ligands [44,45]. The broad peak centered at the wavenumber 3100 cm^{-1} originates from the stretching vibration OH group of water vapor adsorbed on the surface. The peaks were obtained at around 1710 cm-1 due to stretching vibrations of C=O, 1300 cm-1 due to -OH stretching in water molecules present, and around 1000 cm^{-1} due to C-O stretching vibration [41].

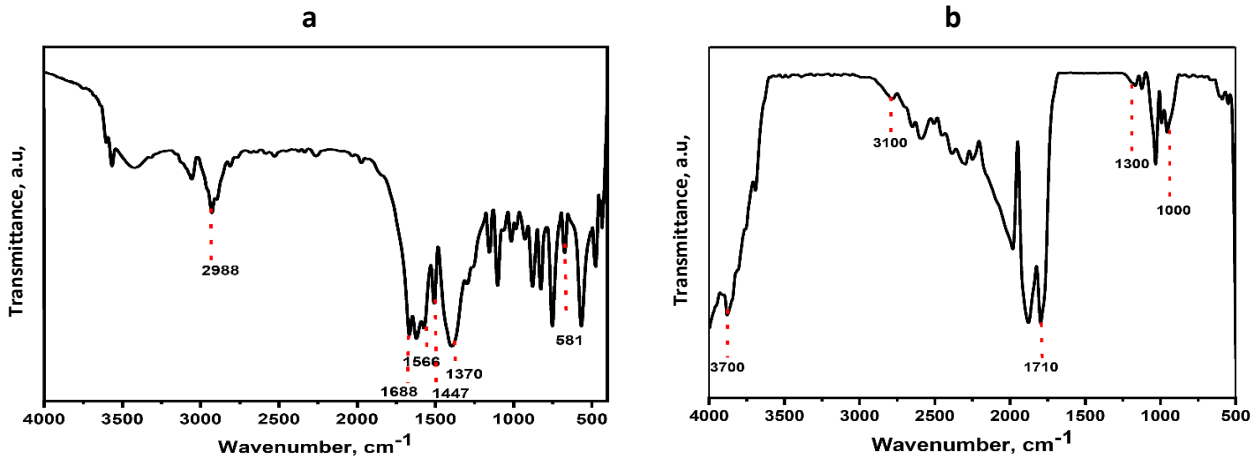

Figure 3. *FTIR plots between 500 to 4000 cm^{-1} for Cu-bdc (a) and Co-bdc (b) MOFs*

Cyclic voltammetry

In order to assess the electrochemical characteristics of the synthesized Co-bdc and Cu-bdc materials, a three-electrode setup was used.

The CV patterns depicted in Figure 4(a) for Co-bdc and Figure 4(b) for Cu-bdc clearly demonstrate that the metal centers had an influence on the electrochemical performance of both MOFs. The voltage range for each electrode material was different. Figure 4(a), it can be observed that Co-bdc displays electrochemical double-layer capacitor (EDLC) behavior within the voltage range of -0.5 to 0 V. It implies that the material intends to undergo more favorable electrochemical reactions at negative potentials. The nearly symmetrical shape and broader CV region indicate a characteristic electrochemical reaction that exhibits high reversibility. The CV profile of Cu-bdc (voltage range of -0.5 to 0.5 V) is shown in Figure 4(b). All of the CV profiles for both the MOFs had quasi-rectangular

shapes, and there were no noticeable shape changes as the scan rate increased, confirming optimal charge-discharge characteristics and outstanding reversibility in the test conditions.

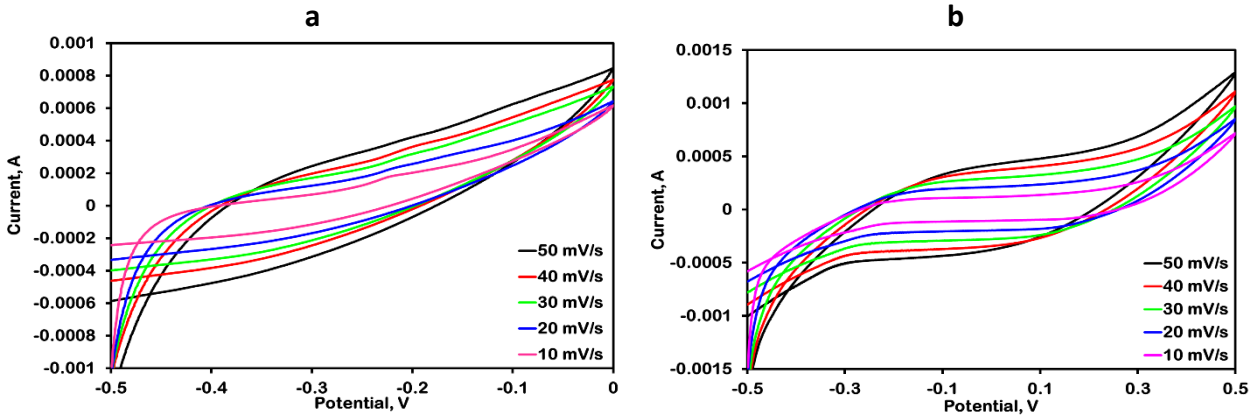

Figure 4. *Cyclic voltammetry profiles of Co-bdc MOF within a potential window of -0.5 to 0 V (a) and Cu-bdc MOF within a potential window of -0.5 to 0.5 V (b), both recorded at a scan rate of 10-50 mV/s*

Electrochemical impedance spectroscopy

The Nyquist plots of Co-bdc and Cu-bdc MOFs are given in Figure 5 (a and b), and the EIS measurements were performed in the 100 kHz to 0.01 Hz frequency range. In Table 1, the values for solution resistance (R_s) and charge transfer resistance (R_{ct}) are displayed. These values suggest a strong potential for high charge transfer capacity and enhanced electronic conductivity in the material or device. The R_s values for the Cu-bdc and Co-bdc electrodes are 1.25 and 0.089 Ω, respectively, as can be deduced from Table 2. The results clearly indicate that the Co-bdc electrode exhibits a reduced R_s value, implying enhanced conductivity and improved wettability. This suggests improved contact between the electrode and the electrolyte solution, facilitating more efficient electrochemical reactions. Lower resistance allows for efficient ion transport, enabling faster kinetics and improved performance in terms of charge/discharge rates. The reduced charge transfer resistance and solution resistance of the Co-bdc electrode would contribute to its higher capacitance value when compared to the Cu-bdc electrode. The accuracy of the results is checked by fitting the impedance data with an appropriate circuit model to assess the accuracy of the measurements. The goodness of fit is examined by statistical measure such as χ^2 values. A low value of χ^2 indicates the chosen circuit model accurately represents the electrochemical process. The circuit used for the fit was $R(CR)W$, where the R_s stands for the solution resistance, R_{ct} for charge transfer resistance, C_{dl} for interfacial double layer capacitance and W for diffusion (Warburg) impedance. In the plot, the blue/red marker indicates the measured values of the Co-bdc and Cu-bdc electrodes, respectively, and the black marker indicates the calculated value.

Figure 5(c) indicates the EIS for both the materials after 2000 consecutive cycles. It is evident that there is an increase in the radius of the depressed semicircle for both the MOFs, which reveals a decrease in the interfacial charge transfer between electrode and electrolyte.

Table 2. *EIS resistance data for Cu-bdc and Co-bdc MOFs*

	Cu-bdc MOF	Co-bdc MOF
R_s / Ω	1.25	0.089
R_{ct} / Ω	2.646	2.239
χ^2	0.04027	0.02906

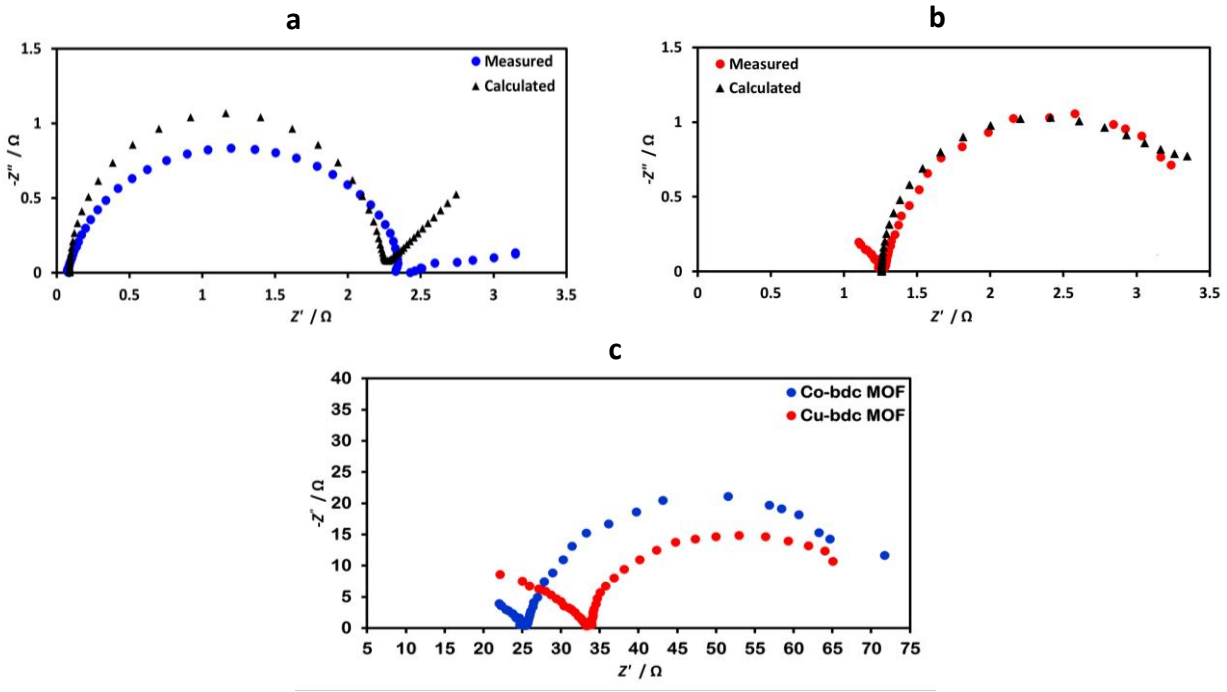

Figure 5. *EIS within a frequency range of 100 kHz to 0.01 Hz of: (a) Cu-bdc MOF; (b) Co-bdc MOF; (c) after 2000 consecutive cycles*

Galvanostatic charge-discharge

The specific capacitance (C_s) of the electrode was calculated using the following equation:

$$C_s = \frac{I\Delta t}{m\Delta V} \tag{1}$$

where I is the charge-discharge current, Δt is the time of discharge, ΔV is the difference between the upper and the lower potential limits, and m is the mass of the material [46].

Figure 6(a) and 6(b) illustrates the GCD curves for Co-bdc and Cu-bdc, respectively. Comparison of the GCD curves of Co-bdc and Cu-bdc electrodes at current densities of 0.5 to 18 A/g reveals a longer discharge time for the Co-bdc electrode, signifying notably larger capacitance for this electrode. Table 3 provides the specific capacitance values and the corresponding voltage drops for Co-bdc and Cu-bdc MOFs at varying current densities. The maximum specific capacitance obtained for Co-bdc MOF and Cu-bdc MOF was 368 and 171 F/g, respectively. It was observed that the voltage drop in the discharge curve rises with increasing applied current density. This escalating voltage drop adversely impacts the accessibility of active sites by ions during electrochemical reactions, leading to a reduction in capacitance. Conversely, at low current density, the voltage drop is minimal, enabling ions to access more active sites, resulting in higher capacitance [47].

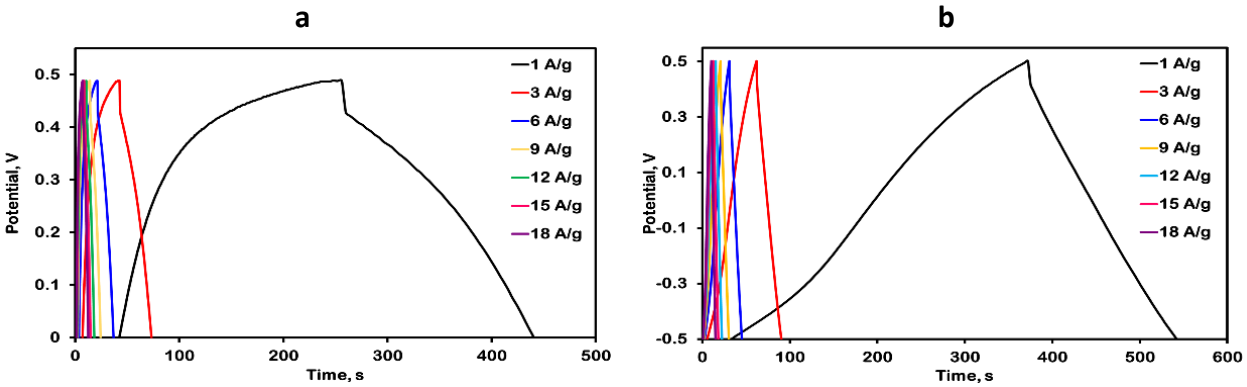

Figure 6. *GCD plots of (a) Co-bdc and (b) Cu-bdc MOF at different current densities ranging from 1 to 18 A/g*

Table 3. *Specific capacitance values of Co-bdc and Cu-bdc MOFs with their corresponding voltage drops at different current densities*

Current density, A/g	Co-bdc MOF		Cu-bdc MOF	
	Voltage drop, mV	Specific capacitance, F/g	Voltage drop, mV	Specific capacitance, F/g
1	32	368	28	171
3	41	199	36	86
6	48	194	44	84
9	62	189	49	81
12	69	187	53	78
15	77	186	55	75
18	81	180	60	72

Cyclic stability and columbic efficiency

The cyclic stability test of the electrodes was carried out using GCD measurement at a current density of 18 A/g for 2000 cycles. Figure 7 shows the capacitance retentions and the columbic efficiency with respect to a number of cycles, while the inset figures show the first 30 charge/discharge cycles for both MOFs. According to the plot presented in Figure 7(a), the Cu-bdc MOF exhibits an impressive retention of approximately 78 % of its initial capacitance after 2000 cycles, even when subjected to a high current density of 18 A/g. This highlights the excellent cyclic stability of the material when utilized as an electrode, even under high-current conditions. Similarly, Figure 7(b) illustrates that the Co-bdc MOF maintains 85 % of its initial capacitance after 2000 cycles at a notable current density of 18 A/g, further emphasizing its stable performance as an electrode material. This suggests that the electrode fabricated using Co-bdc MOF exhibits a longer cycle life and electrochemical reversibility as compared to the Cu-bdc MOF in the 3M KOH electrolyte system. The decrease in capacitance over a period for both MOFs could be attributed to the loss of active material during the cycling process.

Figure 7(a) displays the device coulombic efficiency of Cu-bdc MOF, computed using Eq. (2). The graph indicates consistent stability, hovering around 96 % across the varying number of cycles. This suggests that the charge acquired during the charging phase equals the amount lost during discharging, and notably, this proportion remains constant despite the increasing number of cycles. In Figure 7(b), the coulombic efficiency for Cu-bdc MOF is depicted, revealing a steadfast stability at 98 % over the observed cycles.

The coulombic efficiency (η), which allows us to evaluate the reversibility of the charge/discharge processes, was calculated from Eq. (2):

$$\eta = \frac{t_d}{t_c} 100 \qquad (2)$$

where t_d is the time of discharge and t_c is the time of charge [47].

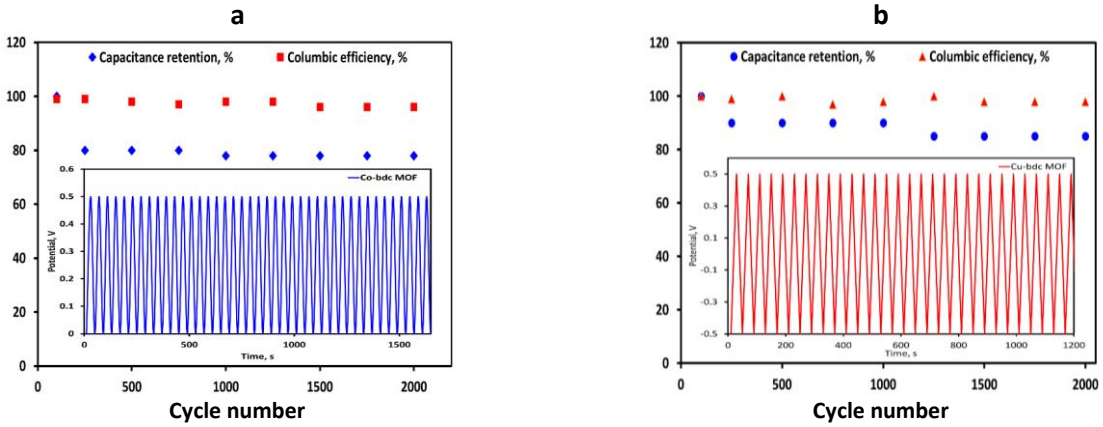

Figure 7. *Cyclic stability test at 18 A/g of (a) Co-bdc and (b) Cu-bdc MOF*

Conclusion

In this study, a facile and environmentally friendly method was employed to synthesize two distinct MOFs, Co-bdc and Cu-bdc MOF, respectively. The MOFs synthesis employed a common ligand material and a nearly identical procedure. The successful synthesis of the MOFs was confirmed through various characterizations, including SEM-EDX, FTIR, and XRD analyses. The goal of this study was to streamline the material synthesis process, emphasizing simplicity and reduced labor, with the aim of minimizing production time and material costs. Then, both materials were compared for their efficiency within the same electrolyte system for supercapacitor applications. Among both MOFs, Cu-bdc MOF demonstrated minimal solution and charge transfer resistance, effectively shortening diffusion paths and facilitating rapid ion transport, leading to exceptional rate performance and long-term stability. The Co-bdc MOF and Cu-bdc MOF exhibited the highest specific capacitance values of 368 and 171 F/g at 1 A/g. Cyclic stability and coulombic efficiency were also evaluated over various cycles, with both MOFs demonstrating outstanding cycling properties and stability. However, the Co-bdc MOF outperformed its counterpart in terms of overall performance for supercapacitor application for a 3M KOH electrolyte system.

***Acknowledgements**: The authors are thankful to the Department of Chemical Engineering, NIT Raipur, Chhattisgarh, India for their support.*

References

[1] J. R. Miller, P. Simon, Electrochemical capacitors for energy management, *Science* **321** (2008) 651-652. https://doi.org/10.1126/science.1158736

[2] P. Simon, Y. Gogotsi, Materials for electrochemical capacitors, *Nature Materials* **7** (2008) 845-854. https://doi.org/10.1038/nmat2297

[3] S. G. Sayyed, M. A. Mahadik, A. V. Shaikh, J. S. Jang, H. M. Pathan, Nano-metal oxide based supercapacitor via electrochemical deposition, *ES Energy & Environment* **3** (2019) 25-44. https://doi.org/10.30919/esee8c211

[4] A. R. Ansari, S. A. Ansari, N. Parveen, M. O. Ansari, Z. Osman, Ag nanoparticles anchored reduced graphene oxide sheets@ nickel oxide nanoflakes nanocomposites for enhanced capacitive performance of supercapacitors, *Inorganic Chemistry Communications* **150** (2023) 110519. https://doi.org/10.1016/j.inoche.2023.110519

[5] S. A. Ansari, Graphene quantum dots: novel properties and their applications for energy storage devices *Nanomaterials* **12(21)** (2022) 3814. https://doi.org/10.3390/nano12213814

[6] F. Zhu, W. Liu, Y. Liu, and W. Shi, Construction of porous interface on CNTs@ NiCo-LDH core-shell nanotube arrays for supercapacitor applications, *Chemical Engineering Journal* **383** (2020) 123150. https://doi.org/10.1016/j.cej.2019.123150

[7] G. Srikesh, A. Samson Nesaraj, Wet Chemical Synthesis of Graphene Containing Co/Mn Co-doped NiONanocrystalline Materials: Efficient Electrode for Electrochemical Supercapacitors, *Iranian Journal of Chemistry and Chemical Engineering* **40(5)** (2021) 1406-1413. https://doi.org/10.30492/ijcce.2020.40537

[8] N. Parveen, G. M. Alsulaim, S. A. Alsharif, H. H. Almutairi, H. A. Alali, S. A. Ansari, M. M. Ahmad Renewable biopolymer-derived carbon–nickel oxide nanocomposite as an emerging electrode material for energy storage applications, *Journal of Science: Advanced Materials and Devices* **8(3)** (2023) 100591. https://doi.org/10.1016/j.jsamd.2023.100591

[9] F. Arshad, N. Parveen, S. A. Ansari, J. A. Khan, M. P. Sk, Renewable biopolymer-derived carbon–nickel oxide nanocomposite as an emerging electrode material for energy storage applications, *Environmental Science and Pollution Research,* **30(28)** (2023) 71464-71471. https://doi.org/10.1007/s11356-022-22626-4

[10] D. D. Babu, M. Mathew, S. Thomas, Supercapacitors based on MXenes (transition metal carbides and nitrides) and their hybrids, *Fundamentals and Supercapacitor Applications of 2D Materials* (2021) 217-233. https://doi.org/10.1016/B978-0-12-821993-5.00006-6
[11] S. Krishnan, A. K. Gupta, M. K. Singh, N. Guha, D. K. Rai, Nitrogen-rich Cu-MOF decorated on reduced graphene oxide nanosheets for hybrid supercapacitor applications with enhanced cycling stability, *Chemical Engineering Journal* **435** (2022) 135042. https://doi.org/10.1016/j.cej.2022.135042
[12] H. García, S. Navalón (Eds.), *Metal-organic frameworks: Applications in separations and catalysis,* John Wiley & Sons, 2018. ISBN: 978-3-527-34313-3
[13] L. He, W. Li, Z. W. Jiang, T. T. Zhao, Y. Li, C. M. Li, Y. F. Li. Novel solvent-triggered transformation of Cu-based metal-organic gels to highly monodisperse metal-organic frameworks with controllable shapes, *Chemical Engineering Journal* **374** (2019) 1231-1240. https://doi.org/10.1016/j.cej.2019.06.026
[14] S. Wang, S. Tang, Rapid and facile synthesis of metal organic framework materials by reaction crystallization in supercritical CO_2, *Materials Letters* **251** (2019) 65-68. https://doi.org/10.1016/j.matlet.2019.05.038
[15] S. A. Tirmizi, A. Badshah, H. M. Ammad, M. Jawad, S. M. Abbas, U. A. Rana S. U. D. Khan, Synthesis of highly stable MOF-5@ MWCNTs nanocomposite with improved hydrophobic properties, *Arabian Journal of Chemistry* **11** (2018) 26-33. https://doi.org/10.1016/j.arabjc.2017.01.012
[16] J. Klinowski, F. A. A. Paz, P. Silva, J. Rocha, Microwave-assisted synthesis of metal–organic frameworks, *Dalton Transactions* **40** (2011) 321-330. https://doi.org/10.1039/C0DT00708K
[17] D. W. Jung, D. A. Yang, J. Kim, J. Kim, and W. S. Ahn, Facile synthesis of MOF-177 by a sonochemical method using 1-methyl-2-pyrrolidinone as a solvent, *Dalton Transactions* **39** (2010) 2883-2887. https://doi.org/10.1039/B925088C
[18] H. M. Yang, L. I. U. Xian, X. L. Song, T. L. Yang, Z. H. Liang, C. M. Fan, In situ electrochemical synthesis of MOF-5 and its application in improving photocatalytic activity of BiOBr, *Transactions of Nonferrous Metals Society of China* **25** (2015) 3987-3994. https://doi.org/10.1016/S1003-6326(15)64047-X
[19] N. L. Rosi, J. Kim, M. Eddaoudi, B. Chen, M. O'Keeffe, O. M. Yaghi. Rod packings and metal–organic frameworks constructed from rod-shaped secondary building units, *Journal of the American Chemical Society* **127(5)** (2005) 1504-1518. https://doi.org/10.1021/ja045123
[20] R. Nivetha, J. Jana, S. Ravichandran, H. N. Diem, T. Van Phuc, J. S. Chung, S. H. Hur, Two-dimensional bimetallic Fe/M-(Ni, Zn, Co and Cu) metal organic framework as efficient and stable electrodes for overall water splitting and supercapacitor applications, *Journal of Energy Storage* **61** (2023) 106702. https://doi.org/10.1016/j.est.2023.106702
[21] T. Sivam, N. S. K.Gowthaman, H. N. Lim, Y. Andou, P. Arul, E. Narayanamoorthi, S. A. John, Tunable electrochemical behavior of dicarboxylic acids anchored Co-MOF: Sensitive determination of rutin in pharmaceutical samples, *Colloids and Surfaces A: Physicochemical and Engineering Aspects* **622** (2021) 126667. https://doi.org/10.1016/j.colsurfa.2021.126667
[22] A. Ehsani, S. Nejatbakhsh, A. M. Soodmand, M. E. Farshchi, H. Aghdasinia, High-performance catalytic reduction of 4-nitrophenol to 4-aminophenol using M-BDC (M= Ag, Co, Cr, Mn, and Zr) metal-organic frameworks, *Environmental Research* **227** (2023) 115736. https://doi.org/10.1016/j.envres.2023.115736
[23] G. Zhan, L. Fan, F. Zhao, Z. Huang, B. Chen, X. Yang, S. F. Zhou, Fabrication of Ultrathin 2D Cu-BDC Nanosheets and the Derived Integrated MOF Nanocomposites, *Advanced Functional Materials* **29(9)** (2019) 1806720. https://doi.org/10.1002/adfm.201806720

[24] G. Zheng, Z. Xing, X. Gao, C. Nie, Z. Xu, Z. Ju, Fabrication of 2D Cu-BDC MOF and its derived porous carbon as anode material for high-performance Li/K-ion batteries, *Applied Surface Science* **559** (2021) 149701. https://doi.org/10.1016/j.apsusc.2021.149701
[25] S. Sadjadi, F. Koohestani, Palladated composite of Cu-BDC MOF and perlite as an efficient catalyst for hydrogenation of nitroarenes, *Journal of Molecular Structure* **1250** (2022) 131793. https://doi.org/10.1016/j.molstruc.2021.131793
[26] S. Rostamnia, H. Alamgholiloo, X. Liu, Pd-grafted open metal site copper-benzene-1, 4-dicarboxylate metal organic frameworks (Cu-BDC MOF's) as promising interfacial catalysts for sustainable Suzuki coupling, *Journal of Colloid and Interface Science* **469** (2016) 310-317. https://doi.org/10.1016/j.jcis.2016.02.021
[27] N. Y. Nikravesh, M. Beygzadeh, M. Adl, Microporous MOF-5@ AC and Cu-BDC@ AC Composite Materials for Methane Storage, *International Journal of Energy Research* **2023** (2023) 2282746. https://doi.org/10.1155/2023/2282746
[28] R. S. Salama, S. A. El-Hakam, S. E. Samra, S. M. El-Dafrawy, A. I. Ahmed, Adsorption, equilibrium and kinetic studies on the removal of methyl orange dye from aqueous solution by using of copper metal organic framework (Cu-BDC), *International Journal of Modern Chemistry* **10(2)** (2018) 195-207.
[29] M. K. Singh, A. K. Gupta, S. Krishnan, N. Guha, S. Marimuthu, D. K. Rai, A new hierarchically porous Cu-MOF composited with rGO as an efficient hybrid supercapacitor electrode material *Journal of Energy Storage* **43** (2021) 103301. https://doi.org/10.1016/j.est.2021.103301
[30] S. Krishnan, A. K. Gupta, M. K. Singh, N.Guha, D. K. Rai, Nitrogen-rich Cu-MOF decorated on reduced graphene oxide nanosheets for hybrid supercapacitor applications with enhanced cycling stability, *Chemical Engineering Journal* **435** (2022) 135042. https://doi.org/10.1016/j.cej.2022.135042
[31] A. K. Gupta, M. Saraf, P. K. Bharadwaj, S. M. Mobin, Dual functionalized CuMOF-based composite for high-performance supercapacitors, *Inorganic Chemistry* **58** (2019) 9844-9854. https://doi.org/10.1021/acs.inorgchem.9b00909
[32] Z. Neisi, Z. Ansari-Asl, A. S. Dezfuli, Polyaniline/Cu (II) metal-organic frameworks composite for high performance supercapacitor electrode, *Journal of Inorganic and Organometallic Polymers and Materials* **29** (2019) 1838-1847. https://doi.org/10.1007/s10904-019-01145-9
[33] Z. Maliha, M. Rani, R. Neffati, A. Mahmood, M. Z. Iqbal, A. Shah, Investigation of copper/cobalt MOFs nanocomposite as an electrode material in supercapacitors, *International Journal of Energy Research* **46** (2022) 17404-17415. https://doi.org/10.1002/er.8406
[34] R. Ramachandran, C. Zhao, D. Luo, K. Wang, F. Wang, Synthesis of copper benzene-1, 3, 5-tricarboxylate metal organic frameworks with mixed phases as the electrode material for supercapacitor applications, *Applied Surface Science* **460** (2018) 33-39. https://doi.org/10.1016/j.apsusc.2017.11.271
[35] M. Azadfalah, A. Sedghi, H. Hosseini, Synthesis of nano-flower metal–organic framework/graphene composites as a high-performance electrode material for supercapacitors, *Journal of Electronic Materials* **48** (2019) 7011-7024. https://doi.org/10.1007/s11664-019-07505-y
[36] S. Ghosh, C. K. Maity, G. C. Nayak, H. P. Nayek, A cobalt (II) metal-organic framework featuring supercapacitor application, *Journal of Solid State Chemistry* **282** (2020) 121093 https://doi.org/10.1016/j.jssc.2019.121093
[37] N. S. Punde, C. R. Rawool, A. S. Rajpurohit, S. P. Karna, A. K. Srivastava, Hybrid composite based on porous cobalt-benzenetricarboxylic acid metal organic framework and graphene nanosheets as high performance supercapacitor electrode, *ChemistrySelect* **3** (2018) 11368-11380. https://doi.org/10.1002/slct.201802721

[38] M. Azadfalah, A. Sedghi, H. Hosseini, H. Kashani, Cobalt based metal organic framework/graphene nanocomposite as high performance battery-type electrode materials for asymmetric supercapacitors, *Journal of Energy Storage* **33** (2021) 101925. https://doi.org/10.1016/j.est.2020.101925

[39] R. Yuniasari, F. Amri, S. A. Abrori, N. L. W. Septiani, M. Rezki, M. Z. Fahmi, B. Yuliarto, A graphene-modified Co-BDC metal-organic frameworks (Co-MOF) for electrochemical non-enzymatic glucose sensing, *IOP Conference Series: Materials Science and Engineering* **1045** (2021) 012010. 10.1088/1757-899X/1045/1/012010

[40] R. Khajavian, K. Ghani, Fabrication of $[Cu_2(bdc)_2(bpy)]_n$ thin films using coordination modulation-assisted layer-by-layer growth, *CrystEngComm* **20** (2018) 1546-1552. https://doi.org/10.1039/C7CE02031G

[41] M. Pamei, S. Kumar, A. G. Achumi, A. Puzari, Supercapacitive amino-functionalized cobalt and copper metal-organic frameworks with varying surface morphologies for energy storage, *Journal of Electroanalytical Chemistry* **924** (2022) 116885. https://doi.org/10.1016/j.jelechem.2022.116885

[42] G. Zhan, L. Fan, F. Zhao, Z. Huang, B. Chen, X. Yang, F. Zhou, Fabrication of Ultrathin 2D Cu-BDC Nanosheets and the Derived Integrated MOF Nanocomposites, *Advanced Functional Materials* **29(9)** (2019) 1806720. https://doi.org/10.1002/adfm.201806720

[43] A. Nayak, S. Viegas, H. Dasari, N. Sundarabal, Cu-BDC and Cu_2O Derived from Cu-BDC for the Removal and Oxidation of Asphaltenes: A Comparative Study, *ACS Omega* **7** (2022) 34966-34973. https://doi.org/10.1021/acsomega.2c03574

[44] L. X. Li, D. Xu, X. Q. Li, W. C. Liu, Y. Jia, Excellent fluoride removal properties of porous hollow MgO microspheres, *New Journal of Chemistry* **38** (2014) 5445-5452. https://doi.org/10.1039/C4NJ01361A

[45] A. Ansari, A. Ali, M. Asif, Shamsuzzaman, Microwave-assisted MgO NP catalyzed one-pot multicomponent synthesis of polysubstituted steroidal pyridines, *New Journal of Chemistry* **42** (2018) 184-197. https://doi.org/10.1039/C7NJ03742B

[46] M. da Silva, D. A. de Lima Almeida, S. S. Oishi, A. B. Couto, N. G. Ferreira, From electrode to device characterizations of polyaniline/micro and nanodiamond/carbon fiber as ternary composites applied as supercapacitor, *Journal of Solid State Electrochemistry* **23** (2019) 1871-1885. https://doi.org/10.1007/s10008-019-04297-3

[47] Q. Li, Q. Zhang, C. Liu, J. Sun, J. Guo, J. Zhan, Y. Yao, Flexible all-solid-state fiber-shaped Ni–Fe batteries with high electrochemical performance, *Journal of Materials Chemistry A* **7(2)** (2019) 520-530.-https://doi.org/10.1039/C8TA09822K